A coherent description of thermal radiative devices and its application on the near-field negative electroluminescent cooling

Lin, C.; Wang, B.; Teo, K.H.; Zhang, Z.

TR2018-022 January 2018

Abstract

Using the transimissivity between two thermal reservoirs and the generalized Planck distributions, we describe the devices that use radiative energy transfer between thermal reservoirs in a unified formalism. Four types of devices are distinguished. For power generators that use the temperature difference between reservoirs, photovoltaic (PV) and thermoradiative (TR) devices respectively use the low-temperature photovoltaic cell and high-temperature thermoradiative cell to generate electricity. For active cooling, the electroluminescent (EL) cooling devices apply a forward bias voltage on the object we want to cool, whereas the negative EL cooling devices apply a reversebias voltage to the heat sink. The relationship among these four devices is explicated. The performance of the negative EL cooling is analyzed, both in the Shockley-Queisser (blackbody spectrum and radiative recombination) framework and the near-field enhancement. The "impedance match" condition derived for PV systems is applied to the negative EL devices. One advantageous feature of the negative EL cooling is that it does not apply the voltage to the target object which we want to cool, and the near-field enhancement can apply to various target materials that support the surface resonant modes.

Energy - Journal

A coherent description of thermal radiative devices and its application on the near-field negative electroluminescent cooling

Chungwei Lin, Bingnan Wang, Koon Hoo Teo

Mitsubishi Electric Research Laboratories, 201 Broadway, Cambridge, Massachusetts 02139, USA

Zhuomin Zhang

George W. Woodruff School of Mechanical Engineering, Georgia Institute of Technology, Atlanta, Georgia 30332, USA

Abstract

Using the transimissivity between two thermal reservoirs and the generalized Planck distributions, we describe the devices that use radiative energy transfer between thermal reservoirs in a unified formalism. Four types of devices are distinguished. For power generators that use the temperature difference between reservoirs, photovoltaic (PV) and thermoradiative (TR) devices respectively use the low-temperature photovoltaic cell and high-temperature thermoradiative cell to generate electricity. For active cooling, the electroluminescent (EL) cooling devices apply a forward bias voltage on the object we want to cool, whereas the negative EL cooling devices apply a reverse bias voltage to the heat sink. The relationship among these four devices is explicated. The performance of the negative EL cooling is analyzed, both in the Shockley-Queisser (blackbody spectrum and radiative recombination) framework and the near-field enhancement. The "impedance match" condition derived for PV systems is applied to the negative EL devices. One advantageous feature of the negative EL cooling is that it does not apply the voltage to the target object which we want to cool, and the near-field enhancement can apply to various target materials that support the surface resonant modes.

Preprint submitted to Elsevier *December 8, 2017*

A coherent description of thermal radiative devices and its application on the near-field negative electroluminescent cooling

Chungwei Lin, Bingnan Wang, Koon Hoo Teo

Mitsubishi Electric Research Laboratories, 201 Broadway, Cambridge, Massachusetts 02139, USA

Zhuomin Zhang

George W. Woodruff School of Mechanical Engineering, Georgia Institute of Technology, Atlanta, Georgia 30332, USA

1. Introduction

Usable work can be extracted from two reservoirs maintained at different temperatures. Photovoltaic (PV) [1, 2, 3] and Thermoradiative (TR) [4, 5, 6, 7] devices are two power generators that use photons emitted at different temperatures to generate electricity. PV devices use the low-temperature (low-T) PV cell to generate charge current, whereas TR devices use the high-temperature (high-T) TR cell for power generation. As the energy transfer is mediated by photons, these devices contains no moving parts, allowing the possible stable and long-lived power generators. By reversing the light-to-electricity processes, work can be done to maintain the temperature difference or to cool one of two reservoirs. The electroluminescent (EL) cooling devices apply a forward bias voltage to the target object which we want to cool [8, 9, 10], whereas the negative EL cooling devices [11, 12, 13, 14] apply a reverse bias voltage to the heat sink that increases the thermal removal flux from the target object. Recently proposed "thermophotonic heat pump" [15] can be viewed as a combination of EL and negative EL cooling. As these four devices share the same microscopic physics, any strategy that boosts the performance of one of the devices, say the PV power generator, can be used to enhance the performance of the other three types of devices.

For a general PV power generator [1], the incoming photons of high and low energies are both wasted – photons of energies lower than the bandgap of PV cell (E_g) cannot generate any electrons and holes, whereas photons of energies higher than E_g can produce a voltage no larger than $E_g/|e|$ (e being the electron charge). Therefore the ideal photon emission spectrum is a δ-function peaked slightly above the PV bandgap, with the peak amplitude as strong as possible [3]. In the far-field based devices, the radiative energy transfer is limited by the blackbody spectrum. However, the δ-function spectrum with a strong peak amplitude can be approximately achieved in the near-field Thermophotovoltaic (TPV) [16, 17, 18, 19]. A basic TPV system consists of an emitter and a PV cell [2, 20, 21, 22, 23, 24], with the emitter placed between the heat source and the PV cell. The main role of the emitter is to modify the photon emission spectrum that better fits the bandgap of the PV cell. For the near-field based TPV system [25, 26, 27, 28, 29, 30, 31, 32], the separation between the emitter and the PV cell is much shorter than the characteristic wavelength of the emitted photons, and the resulting photon emission spectrum approaches a δ-function of large amplitude. The strong enhancement stems from the surface resonances supported by the emitter/vacuum interface (surface plasmon polaritons) [16, 33]. Recently, using the framework of Coupled Mode Theory (CMT) [33, 34, 35, 36, 37, 38], Karalis and Joannopoulos show that the performance of the TPV system can be strongly enhanced [32] when the emitter and PV cell are designed, as a whole, to satisfy the "impedance matching" condition derived from CMT [33]. The impedance matching condition for TPV can be stated as follows: if both PV/vacuum and emitter/vacuum by themselves support their respective surface resonances, the radiative energy transfer is maximized when the (complex) resonant energies are identical; if there is only one resonant mode, the radiative energy transfer is maximized when the resonant mode decays to the PV cell and to the emitter at the same rate [33, 37, 39].

In our previous work [40], we describe both PV and TR power generators in a unified formalism that involves the transmissivity between two reservoirs and the generalized Planck distributions [41, 42, 43]. We also showed how near-field TPV concept can enhance the TR performance. In the present work, we further generalize the formalism to all four devices mentioned above, and therefore the "impedance matching" condition derived for TPV can be easily applied to all types of devices. In particular, we focus on the negative EL cooling whose near-field enhancement has not extensively studied in literatures [14]. Only the planar structure is considered, and the transmissivity is computed using the dyadic Green function [44, 45, 46] (see also Appendix) and the fluctuation-dissipation relation between the thermal current and temperature [47]. The rest of the paper is organized as follows. In section 2, we provide a general and unified formalism for thermal radiative devices including PV and TR power generators, as well as the EL and negative EL active cooling devices. We show that the performance of these devices, including the output power and the efficiency, can be expressed in terms of transmissivity and the generalized Planck distribution. A coherent description of these four devices are provided; the reverse saturation current is found to be a good indicator of the near-field effect for all devices. In section 3 we give a few model examples on the negative EL cooling devices, emphasizing the near-field enhancement. The connection between all near-field devices are explicated. Some features and advantages specific to the negative EL cooling are pointed out. Finally a brief conclusion is given in Section 4.

2. General Formalism

2.1. Overview

Four types of devices using radiation energy transfer are illustrated in Fig. 1 – they are PV power generators, TR power generators, EL cooling devices, and negative EL cooling devices. All these devices involve at least two different thermal reservoirs, with each reservoir characterized by a temperature (T) and a chemical potential (μ, or equivalently a bias voltage $|e|V = \mu$). Before providing the formalism that describes all these devices, in Section 2.2 we briefly review the basic description of non-equilibrium electron-hole (e-h) concentrations, the generalized Planck distribution that introduces a non-zero photon chemical potential to describe the e-h generation and recombination, and fix the sign convention of charge current and bias voltage used in this paper. Section 2.3 provides the general formalism for all four devices. Section 2.4 is devoted to the cooling performance, including the "thermophotonic heat pump" [15]. Section 2.5 gives a coherent description of all four devices.

2.2. Quasi-Fermi energies, generalized Planck distribution and sign convention

To describe the electron and hole concentrations away from their equilibrium values, two (quasi) Fermi energies, one for electrons denoted as E_{FC} and one for holes denoted as E_{FV}, are needed [3]. The difference $E_{FC} - E_{FV} = \mu$ defines the photon chemical potential. At equilibrium, two Fermi energies are identical, i.e. $E_{FC} = E_{FV} = E_F$. When the e-h concentration is larger than that at equilibrium (under an illumination or a forward bias), the electron Fermi energy increases ($E_{FC} > E_F$) whereas the hole Fermi energy decreases ($E_{FV} < E_F$), and a positive μ is developed to account for the additional e-h concentration. When the e-h concentration is smaller than that at equilibrium (under a reverse bias), the electron Fermi energy decreases $E_{FC} < E_F$ whereas the hole Fermi energy increases $E_{FV} > E_F$, and a negative μ is developed to account for the reduced e-h concentration. Fig. 2 illustrates the E_{FC}, E_{FV}, and μ under different conditions. We note that, reversely, a photon chemical potential can be *defined* for the steady-state populations that are different from those at thermal equilibrium. This allows analyzing the performance of the molecular light-to-current conversion in the same framework of PV devices [48, 49].

The photon chemical potential is used in the generalized Planck distribution [41, 42, 43] – for a thermal reservoir at a fixed temperature T and a photon chemical potential μ, the mean photon occupation number of the angular frequency ω is

$$\Theta(\omega; T, \mu) = \frac{1}{\exp\left[(\hbar\omega - \mu)/T\right] - 1}, \tag{1}$$

with T the temperature measured in energy, i.e. the Boltzmann constant $k_B \equiv 1$. The photon chemical potential is used to describe $e+h \leftrightarrow \gamma$ processes in the cell (γ labels the photons). In this convention, a positive μ corresponds a larger e-h concentration, implying a larger e-h recombination rate and therefore a larger emitted photon number; a negative μ corresponds a smaller e-h concentration, implying a smaller e-h recombination rate and therefore a smaller emitted photon number. From a fundamental point of view, the use of quasi-Fermi energies *assumes* the electron and hole energy distributions still possess the "Fermi-Dirac" form in the non-equilibrium steady state, based on which the generalized Planck distribution for photons can be derived using the principle of detailed balance [3].

The sign convention is defined with respect to a pn-junction [Fig. 3(a)]. Under a forward bias, the current flows from p-side to n-side, which defines the positive voltage and the positive current. The photo-generated current (photocurrent) is negative in this convention. For a pn-junction, the short-circuit current j_{sc} and the reverse saturation current j_S determine the characteristic of the current-voltage behavior

$$j = j_S \left[e^{|e|V/T} - 1\right] + j_{sc}. \tag{2}$$

$j_{sc} = -|j_{sc}|$ is the photo-generated current, which is negative (see Eq. 6 and Eq. 21 for a derivation). A typical behavior of Eq. 2 is given in Fig. 3(b). Without providing the details, we note $|e|V = \mu$, and the photon chemical potential and the bias voltage can be used interchangeably [3].

Let us discuss the PV devices using Eq. 2. On the one hand, the illumination provides a short-circuit current j_{sc} that is along the reverse bias direction. On the other hand, illumination increases the e-h concentration that develops a forward bias voltage. This voltage-current relation means that the photon current in the pn-junction, as a PV cell, is providing a "negative" power [the red curve of Fig. 3 (b)]. In other words, the photocurrent inside the PV cell flows *against* the voltage which the incident photons generate – the holes flow to the $+|V|$ side and electrons flow to the $-|V|$ side. Once an external load is attached, electrons and holes recombine through the load to produce the electric power.

In the ideal PV cell where only the radiative recombination is considered, the photocurrent (I_c) is equal to the flux difference between the photon absorption (which generates current) and photon emission (which annihilates current). The power is given by

$$P_{cell} = (-I_c) \times V = \frac{-I_c}{|e|} \times \mu, \tag{3}$$

The minus sign comes from that the photocurrent is by definition negative. If P_{cell} is positive, the cell consumes energy; if P_{cell} is negative, the cell generates energy [Fig. 3 (b)].

2.3. The formalism

Now the radiative energy transfer between two reservoirs is considered. A reservoir is characterized by a temperature T and an voltage $|e|V = \mu$. Considering two reservoirs, labeled as 1 and 2, fixed respectively at (T_1, μ_1) and (T_2, μ_2), the photon number flux and energy flux from 1 to 2 are given by

$$\dot{N}_{1\to 2} = \int_0^\infty \frac{d\omega}{2\pi} \varepsilon_{12}(\omega) \left[\Theta(\omega; T_1, \mu_1) - \Theta(\omega; T_2, \mu_2)\right], \tag{4}$$

$$P_{1\to 2} = \int_0^\infty \frac{d\omega}{2\pi} \hbar\omega\varepsilon_{12}(\omega) \left[\Theta(\omega; T_1, \mu_1) - \Theta(\omega; T_2, \mu_2)\right]. \tag{5}$$

Here the transmissivity between the reservoirs 1 and 2 is given as $\varepsilon_{12}(\omega)$ [33]. Eq. 4 and 5 imply that a non-zero chemical potential difference can be generated via a temperature difference or vise versa. The transmissivity $\varepsilon_{12}(\omega)$ is a dimensionless quantity for general geometries. In the planar configurations considered here, however, it is more convenient to compute the transmissivity per unit area. In this case, Eq. 4 and 5 provide the photon number flux density and energy flux density (i.e. flux per unit area). Since systems composed of two reservoirs will be considered, the subscripts will be neglected, i.e., $\varepsilon_{12}(\omega) \equiv \varepsilon(\omega)$, for the rest of the paper.

Four types of devices are now distinguished. The PV devices use the low-T reservoir (PV cell) to generate the power. The photocurrent and its generated power at PV cell is

$$\begin{aligned} I_c &= |e|\dot{N}_{T_h\to T_l} = |e| \int_0^\infty \frac{d\omega}{2\pi} \varepsilon(\omega) \left[\Theta(\omega; T_h, 0) - \Theta(\omega; T_l, \mu)\right], \qquad (6) \\ P_{cell} &= -\mu\dot{N}_{T_h\to T_l} \end{aligned}$$

Here T_h/T_l is the temperature of the high-T/low-T reservoir. When $\mu > 0$ and $\Theta(\omega; T_h, 0) - \Theta(\omega; T_l, \mu) > 0$ (so that $I_c > 0$), the power is "negative", meaning it generates power. Using Eq. 5, the power absorbed by the PV cell is

$$P_{T_h\to T_l} = \int_0^\infty \frac{d\omega}{2\pi}\,\hbar\omega\varepsilon(\omega)\left[\Theta(\omega;T_h,0)-\Theta(\omega;T_l,\mu)\right], \tag{7}$$

which is positive, meaning the PV cell gets energy from the other reservoir.

The TR devices use the high-T reservoir (TR cell) to generate the power. The photocurrent and its generated power at TR cell is

$$\begin{aligned} I_c &= |e|\dot{N}_{T_l\to T_h} = |e|\int_0^\infty \frac{d\omega}{2\pi}\varepsilon(\omega)\left[\Theta(\omega;T_l,0)-\Theta(\omega;T_h,\mu)\right], \\ P_{cell} &= -\mu\dot{N}_{T_l\to T_h} \end{aligned} \tag{8}$$

When $\mu < 0$ and $\Theta(\omega;T_l,0)-\Theta(\omega;T_h,\mu) > 0$ (so that $I_c < 0$), the power is "negative", meaning it generates power. Using Eq. 5, the power absorbed by the high-T TR cell is

$$P_{T_l\to T_h} = \int_0^\infty \frac{d\omega}{2\pi}\hbar\omega\varepsilon(\omega)\left[\Theta(\omega;T_l,0)-\Theta(\omega;T_h,\mu)\right], \tag{9}$$

which is negative, meaning the TR cell losses energy to the other reservoir.

For cooling devices, we assume reservoirs 1 and 2 are at temperatures T_1 and T_2 respectively, and reservoir 1 at T_1 is the target cell which we want to cool; reservoir 2 serves as the heat sink. The EL cooling devices apply a forward bias voltage to the target cell. The photocurrent and its generated power at the target cell is

$$\begin{aligned} I_c &= |e|\dot{N}_{T_2\to T_1} = |e|\int_0^\infty \frac{d\omega}{2\pi}\varepsilon(\omega)\left[\Theta(\omega;T_2,0)-\Theta(\omega;T_1,\mu)\right], \\ P_{cell} &= -\mu\dot{N}_{T_2\to T_1} \end{aligned} \tag{10}$$

When $\mu > 0$ and $\Theta(\omega;T_2,0)-\Theta(\omega;T_1,\mu) < 0$ (so that $I_c < 0$), the power is "positive", meaning the target cell consumes the power. Using Eq. 5, the power absorbed by the target cell is

$$P_{T_2\to T_1} = \int_0^\infty \frac{d\omega}{2\pi}\hbar\omega\varepsilon(\omega)\left[\Theta(\omega;T_2,0)-\Theta(\omega;T_1,\mu)\right], \tag{11}$$

which is negative, meaning the target cell dissipates its heat to heat sink.

The negative EL cooling devices apply a reverse bias voltage to the heat sink. The photocurrent and its generated power at the heat sink is

$$\begin{aligned} I_c &= |e|\dot{N}_{T_1\to T_2} = |e|\int_0^\infty \frac{d\omega}{2\pi}\varepsilon(\omega)\left[\Theta(\omega;T_1,0)-\Theta(\omega;T_2,\mu)\right], \\ P_{cell} &= -\mu\dot{N}_{T_1\to T_2} \end{aligned} \tag{12}$$

When $\mu < 0$ and $\Theta(\omega;T_1,0)-\Theta(\omega;T_2,\mu) > 0$ (so that $I_c > 0$), the power is "positive", meaning the heat sink consumes the power. Using Eq. 5, the power absorbed by the reservoir 2 is

$$P_{T_1\to T_2} = \int_0^\infty \frac{d\omega}{2\pi}\hbar\omega\varepsilon(\omega)\left[\Theta(\omega;T_1,0)-\Theta(\omega;T_2,\mu)\right], \tag{13}$$

which is positive, meaning the heat sink gets thermal radiation energy from the target cell.

2.4. Cooling performance and maximum heat removal flux

For a cooling device, the coefficient of performance or COP is defined by

$$\eta_{COP} = \frac{Q_c}{W} \tag{14}$$

with W being the work done to the device, and Q_c the heat removed from the reservoir of interest. Larger η_{COP} implies a larger heat removal flux for the same input work, or the same heat removal flux at a smaller input work. For EL cooling devices, using Eq. 10 and 11, one gets

$$\eta_{COP,EL} = \frac{-\int_0^\infty \frac{d\omega}{2\pi}\hbar\omega\varepsilon(\omega)\left[\Theta(\omega;T_2,0)-\Theta(\omega;T_1,\mu)\right]}{-\mu\int_0^\infty \frac{d\omega}{2\pi}\varepsilon(\omega)\left[\Theta(\omega;T_2,0)-\Theta(\omega;T_1,\mu)\right]} \tag{15}$$

μ being positive for the EL cooling ensures $\eta_{COP,EL} > 0$. For negative EL cooling devices, using Eq. 12 and 13, one gets

$$\eta_{COP,NEL} = \frac{\int_0^\infty \frac{d\omega}{2\pi}\hbar\omega\varepsilon(\omega)\left[\Theta(\omega;T_1,0)-\Theta(\omega;T_2,\mu)\right]}{-\mu\int_0^\infty \frac{d\omega}{2\pi}\varepsilon(\omega)\left[\Theta(\omega;T_1,0)-\Theta(\omega;T_2,\mu)\right]} \tag{16}$$

μ being negative for the negative EL cooling ensures $\eta_{COP,NEL} > 0$.

In addition to COP, the net radiation flux *leaving* the cell (at T_1), given by the negative of Eq. 11 for the EL cooling and Eq. 13 for the negative

EL cooling, is another important quantity of interest. For the negative EL cooling, there exist a maximum current and a maximum radiation flux

$$I_{c,max} = e\int_0^\infty \frac{d\omega}{2\pi}\varepsilon(\omega)\Theta(\omega;T_1,0) \tag{17}$$

$$P_{TR,max} = \int_0^\infty \frac{d\omega}{2\pi}\hbar\omega\varepsilon(\omega)\Theta(\omega;T_1,0) \tag{18}$$

because $\Theta(\omega;T_2,\mu) \to 0$ as $\mu \to -\infty$. To have a larger cooling power, Eq. 18 should be as large as possible, and increasing the transmissivity $\varepsilon(\omega)$ is the key to enhance the cooling performance. The dimension of Eq. 13 is power per unit area, and can be used as the boundary condition when we use the Fourier law (thermal conductivity) to compute the temperature distribution within the cell. We emphasize that the current description only concerns the radiative processes, and thus represents the ideal condition. In the next subsection we shall briefly describe how to take the non-radiative processes into account.

Within our framework, the "thermophotonic heat pump" (THP) proposed by Oksanen and Tulkki [15] can be formulated as a combination of EL and negative EL cooling. It requires two semiconductors – one serves as the object one wants to cool with a forward bias $\mu_1 > 0$; the other as the heat sink with a reverse bias $\mu_2 < 0$. Assuming their respective temperatures are T_1 and T_2, the COP is

$$\eta_{COP,THP} = \frac{\int_0^\infty \frac{d\omega}{2\pi}\hbar\omega\varepsilon(\omega)\left[\Theta(\omega;T_1,\mu_1)-\Theta(\omega;T_2,\mu_2)\right]}{(\mu_1-\mu_2)\int_0^\infty \frac{d\omega}{2\pi}\varepsilon(\omega)\left[\Theta(\omega;T_1,\mu_1)-\Theta(\omega;T_2,\mu_2)\right]}, \tag{19}$$

and the maximum heat removal flux is $\int_0^\infty \frac{d\omega}{2\pi}\hbar\omega\varepsilon(\omega)\Theta(\omega;T_1,\mu_1)$. Note that THP devices also work when $\mu_2 > 0$ (but $\mu_1 > \mu_2$ to ensure positive work), and in this sense THP is more general than the combination of EL and negative EL cooling.

2.5. A coherent description of all four types of devices

We conclude this section by discussing the performance using the voltage-current relations of all four devices. When the Planck distributions are approximated by the corresponding Boltzmann distributions, $-I_c$ in Eq. 6 and

Eq. 8 respectively reduce to

$$\begin{aligned} -I_c \equiv j_{PV}(V) &= |e| \int_0^\infty \frac{d\omega}{2\pi} \varepsilon(\omega) e^{-\hbar\omega/T_l}(e^{|e|V/T_l} - 1) \\ &+ |e| \int_0^\infty \frac{d\omega}{2\pi} \varepsilon(\omega)[e^{-\hbar\omega/T_l} - e^{-\hbar\omega/T_h}], \end{aligned} \tag{20}$$

$$\begin{aligned} -I_c \equiv j_{TR}(V) &= |e| \int_0^\infty \frac{d\omega}{2\pi} \varepsilon(\omega) e^{-\hbar\omega/T_h}(e^{|e|V/T_h} - 1) \\ &- |e| \int_0^\infty \frac{d\omega}{2\pi} \varepsilon(\omega)[e^{-\hbar\omega/T_l} - e^{-\hbar\omega/T_h}]. \end{aligned} \tag{21}$$

Eq. 2 is thus obtained by identifying

$$j_S = |e| \int_0^\infty \frac{d\omega}{2\pi} \varepsilon(\omega) e^{-\hbar\omega/T_l} > 0, \tag{22}$$

$$j_{sc} = |e| \int_0^\infty \frac{d\omega}{2\pi} \varepsilon(\omega)[e^{-\hbar\omega/T_l} - e^{-\hbar\omega/T_h}] < 0. \tag{23}$$

Both $j_{PV}(-\infty)$ and $j_{TR}(-\infty)$ are negative. When using the same T_h and T_l, $j_{PV}(0) = -j_{TR}(0) = -j_{sc} < 0$. The voltage-current (V-I) relations for PV and TR devices are respectively illustrated in red and in blue in Fig. 3 (b). When $T_h = T_l$, $j_{sc} = 0$ and $j_{PV}(V) = j_{TR}(V) = j_S(e^{|e|V/T_l} - 1)$, recovering the voltage-current relation of a pn-junction in the dark [50]. Note that the reverse saturation current j_S depends on $\varepsilon(\omega)$ and thus can be used as a quantity to characterize the near-field effect *without* maintaining the temperature difference and a vacuum gap between two reservoirs.

The PV power generators work in the $0 < V < V_{oc}^{PV}$ range of $j_{PV}(V)$ [red curve in Fig. 3 (b)], whereas the TR power generators work in the $V_{oc}^{TR} < V < 0$ range of $j_{TR}(V)$ [blue curve in Fig. 3 (b)]. The output power of the PV and TR power generators are shown as the blue shaded areas in Fig. 3 (b). Certainly one wants the output power as large as possible. The EL cooling devices work in the $V > V_{oc}^{PV}$ range of $j_{PV}(V)$ [red curve in Fig. 3 (b)], whereas the negative EL cooling devices work in the $V < V_{oc}^{TR}$ range of $j_{TR}(V)$ [blue curve in Fig. 3 (b)]. The work done to the EL and negative EL devices are shown as the areas of dashed boxes in Fig. 3 (b). To have a larger COP of cooling devices, for a given heat removal flux, the work done to the cooling devices should be as small as possible.

It is worth emphasizing that both V-I curves in Fig. 3 (b) can be obtained from measuring/computing the *same* physical device, which implies that the same physical device can be used for different purposes, depending on the applied voltage and temperature. Inclusions of non-radiative processes modify the V-I relations, and its implications on PV and TR devices will be presented elsewhere. Table 1 summarizes the function and the working parameters of all four devices. Four types of devices work at four different quadrants defined by the $(\mu, -I_c)$ plane. PV power generators and EL cooling devices work at $\mu > 0$, whereas TR power generators and negative EL cooling devices work at $\mu < 0$. When only the radiative recombination is considered, $\mu > 0$ devices generally have larger output powers (larger output power for power generators and larger heat removal flux for the cooling devices) than $\mu < 0$ devices.

3. Near-field enhancement on the negative electroluminescent cooling

3.1. Overview and material parametrization

In this section we apply the formalism to the negative EL cooling devices, emphasizing the near-field enhancement. The same analysis on other three devices are given in our previous work [39, 40]. The basic components of a negative EL cooling device is illustrated in Fig. 4(a). The heat sink is a semiconductor, characterized by a bandgap E_g. Applying a reverse bias to the heat sink reduces the photon emission of the heat sink, effectively enhancing the heat removal flux of the object one wants to cool. We choose the heat sink to be a semiconductor of $E_g = 0.2$ eV, whose temperature varies from $T_s = 320$ K to $T_s = 380$ K. 0.2 eV is roughly the bandgap of InSb [51, 52]. The cell to be cooled, the target cell, is fixed at $T_c = 350$ K, and its dielectric property will be specified shortly. We consider the semi-infinite target cell and heat sink are separated by $d = 20$ nm. The goal is to see how much heat flux can be removed from the cell when a reverse bias voltage is applied to the semiconductor heat sink.

For the semiconductor heat sink, the dielectric function is governed by the direct valence-to-conduction interband transition [53, 54],

$$\epsilon_{pv}(\omega) \quad = \quad \epsilon_r(\omega) + i\epsilon_i(\omega) \tag{24}$$

$$\begin{aligned}\epsilon_i(\omega) &= A\sqrt{x-1}/x^2, \;\; x > 1 \\ &= 0, \;\; x < 1 \\ \epsilon_r(\omega) &= B + A(2 - \sqrt{1+x})/x^2, \;\; x > 1 \\ &= B + A(2 - \sqrt{1+x} - \sqrt{1-x})/x^2, \;\; x < 1.\end{aligned}$$

with $x = \hbar\omega/E_g$. As a model calculation, we use $(A, B, E_g) = (6, 10, 0.2 \text{ eV})$ [16]. We have varied A and B between 1 and 15 extracted from Refs. [53, 54], and found that they do not noticeably change the general behavior. The material of the dielectric functions of Eq. 25 will be referred to as "interband" material.

Three types of target cells are considered: the metal, the Lorentz material, and the same interband material as the heat sink, with the blackbody as the reference. Both metal and Lorentz material support the surface plasmon polariton mode with a (surface) plasma frequency ω_0. Our parameter choice is guided by the impedance matching condition [39, 40]: a large transmissivity can be obtained when the resonant energy $\hbar\omega_0$ is slightly larger than the bandgap E_g. We therefore use $\hbar\omega_0 = 1.1 \cdot E_g$. The effect of decay rate will be discussed in the next subsection. For the metal target cell, the dielectric function can be approximated by the Drude model:

$$\epsilon_m = 1 - \frac{\omega_{pl}^2}{\omega^2 + i\gamma_m\omega}. \tag{25}$$

The surface resonant frequency is given by $\omega_0 = \omega_{pl}/\sqrt{2}$, so we choose $\omega_{pl} = \sqrt{2} \times 1.1 \cdot E_g$, and the decay is chosen to be $\gamma_m = 0.002\omega_{pl}$. For the Lorentz target cell, the dielectric function can be described by the Lorentz oscillator model:

$$\epsilon_L(\omega) = \epsilon_\infty \frac{\omega^2 - \omega_{LO}^2 + i\gamma\omega}{\omega^2 - \omega_{TO}^2 + i\gamma\omega}. \tag{26}$$

This is typical for many insulators. Here we choose $\epsilon_\infty = 4.46$. $\omega_{TO}/\omega_{LO} = 0.81$ and $\gamma/\omega_{LO} = 0.0041$. The resonant frequency is given by $\omega_0^2 = \frac{\omega_{LO}^2 + \omega_{TO}^2/\epsilon_\infty}{1+1/\epsilon_\infty}$, which is set to $(1.1 \cdot E_g/\hbar)^2$. The third choice is inspired by its symmetric configuration, which is shown to greatly enhance the transmissivity for both metal and Lorentz materials [16, 33, 39, 40]. For the blackbody reference, the emissivity is given by [33, 40]

$$\varepsilon_{c,s}(\omega) = \frac{1}{2\pi}(\frac{\omega}{c})^2\Theta(\omega - E_g/\hbar). \tag{27}$$

3.2. Simulation results

Fig. 4(b)-(d) show the input power (done to the heat sink) and the heat removal flux (per unit area) for various target cells, with the blackbody reference. The target cell is fixed at $T_c = 300$ K, whereas the heat sink varies from $T_s = 250$, 300, and 350 K. Some general features are pointed out. We first consider the case with zero bias voltage. When $T_s = T_c$, the target cell and the heat sink are in equilibrium and there is no outgoing radiative flux from the target cell; When $T_s > T_c$, the heat sink emits more photons than the target cell such that the outgoing radiative flux from the target cell is negative (heating); When $T_s < T_c$, the heat sink emits less photons than the target cell such that the outgoing radiative flux from the target cell is positive (cooling). When applying the reverse bias voltage, the heat removal flux increases as the heat sink emits less photons, and reaches a saturation flux given in Eq. 18. Note that when the heat sink is fixed at a higher temperature ($T_s > T_c$), a minimum applied voltage amplitude ($V < 0$) is needed for cooling to happen. In our near-field arrangement (20 nm separation between the planar target cell and the heat sink), the enhancement of the heat removal flux is about 63 times (for the metal target cell), 22 times (for the Lorentz target cell), and 11 times (for the same interband target cell) larger than the blackbody reference. These results are comparable to the enhancement of the TR power generator devices [40]. In the model simulations considered here, the outgoing radiative flux saturates when $|eV|$ is about 10-20% of the bandgap E_g. The COP (η_{COP}) are computed using Eq. 16, and the results for $T_s = 300$ K/250 K, $T_c = 300$ K are given in Fig. 5. Generally, the COP for all target types of target cells are very close in value. The target cells that support surface resonances, i.e., metal and Lorentz, have a COP about 5% lower than those that do not support surface resonances i.e., interband and blackbody. This qualitative feature is found for other choices of $T_s \neq T_c$ [see Fig. 5(a) and (b)].

For metal and Lorentz target cells, the strong near-field enhancement originates from surface resonances introduced by the metal/vacuum and

Lorentz/vacuum interfaces. The energies of surface modes lie within a small energy window [39]. In the far-field setup, the surface modes do not contribute to the radiative energy transfer due to the exponential decay in the out-of-plane direction. In the near-field setup, the surface modes produce a δ-function like peak with a strong peak amplitude in transimissivity and greatly increase the radiative energy transfer [40]. An interesting and perhaps non-intuitive consequence derived from impedance matching condition is that the damping of the resonance can sometimes help the radiative energy transfer. In other words, there exists an optimal damping value for the maximum radiative energy transfer. This is explicitly shown in PV [32] and TR [40] devices. To illustrate this effect on negative EL cooling devices, Fig. 6 shows the outgoing radiative fluxes per unit area for the metals with plasma damping rate $\gamma_e/\omega_{pl} = 0.002$, 0.004, 0.016, and 0.030 for two temperature differences. The radiative flux indeed shows a maximum value when $\gamma_m/\omega_{pl} \sim 0.016$, above and below which the radiative flux decreases.

3.3. Discussion

We begin the discussion by comparing the TR devices as a power generator with the negative EL cooling (two $\mu < 0$ devices, see Table. 1). Both power generators and cooling devices require attaching an external load to one of the reservoirs, which is a semiconductor whose dielectric function is approximated by the interband material in Eq. 25 – for TR power generators it is the TR cell that generates electricity; for the negative EL cooling it is the heat sink that uses the input power for cooling. For TR power generators one chooses a heat sink to maximize the output power for a given TR cell, whereas for the negative EL cooling devices one selects a target cell for a given heat sink. In essence, we want to increase the radiative power transfer from one reservoir to the other. Within the formalism given in Eq. 4 and 5, the key is to design (via the material selection and their geometry) two reservoirs (e.g. the target cell and heat sink for the negative EL cooling) simultaneously that maximizes their mutual transmissivity, and the impedance-matching condition derived from CMT provides a very good guidance [33, 39]. These considerations are general for PV devices as well. As the transimissivity determines the near-field performance, it could be a good experimental quantity to measure.

Two advantages of negative EL cooling devices are worth noting. First it does not apply a voltage to the target cell which we want to cool, allowing more material choices of target cell. In contrast, the EL cooling requires a p-doped region, an n-doped region, and a bias voltage to the target cell, which has to be a semiconductor [8, 10]. Second, as the negative EL devices aim to reduce the e-h concentrations in the heat sink, the Auger recombination, which typically suppresses the PV and TR performances, becomes less significant. Potential applications for the negative EL cooling include to cool the wide-gap insulator (e.g. SiC, BN) that supports the surface polariton (optical phonons) using a small-bandgap semiconductor as a heat sink, and to cool a metal using a semiconductor heat sink whose bandgap is comparable to the metal/vacuum surface plasma energy. Finally we emphasize again that any approaches that enhance the TPV performance, such as coating the PV cell or coating the emitter [39], can be applied to the negative EL cooling.

Finally, we recognize that the near-field devices, such as the setup in Fig. 4(a), are experimentally very challenging. First, to maintain a small vacuum gap between the target cell and the heat sink is difficult, and one possible solution is to use a few short supports to separate the target cell and the heat sink [55, 56, 57]. Second, to fabricate a P-I-N junction in the heat sink is also difficult. Combining some thin film fabrication methods [58, 59, 60] to diffusion driven charge transport structures [61, 62, 63, 64] can potentially make the device. However, if not properly passivated, the resulting large surface recombination can outweigh the near-field gain.

4. Conclusion

To conclude, we provide a coherent formalism that applies to all devices that use radiative energy transfer for the power generation and the active cooling. The formalism includes the generalized Planck distribution that characterizes a thermal reservoir by a temperature and a chemical potential, and the transmissivity between the cell (that generates power or is to be cooled) and its corresponding heat source or heat sink. In this framework, four types of devices are distinguished: a PV device that uses the low-temperature reservoir to generate electricity; a TR device that uses the high-temperature reservoir to generate electricity; an EL device that applies a voltage to the cell to be cooled; a negative EL device that applies a voltage to the heat sink. In all these devices, the transimissivity is the material and geometry specific quantity that plays the crucial role in the performance. Once the "impedance match" condition, originally derived for optimizing PV devices, is formulated using transmissivity, it can be straightforwardly generalized to other types of devices. Using the formalism, we analyze the performance of the negative EL cooling, in the Shockley-Queisser framework as a reference and its near-field enhancement. For the near-field arrangement, a small bandgap semiconductor is chosen as the heat sink, which is close to the target cell which we want to cool. The heat removal flux can be more than ten times larger than the blackbody reference. As the negative EL cooling applies the voltage on the heat sink instead of the target cell (which we want to cool), it can be useful for cooling the wide-gap insulators or metals.

Acknowledgement

We thank anonymous reviewers for pointing out the "thermophotonic heat pump" and a few technological challenges for near-field devices. Z.M.Z. would like to thank the support from the U.S. Department of Energy, Office of Science, Basic Energy Sciences (Grant Nos. DE-FG02-06ER46343 and DE-SC0018369).

Appendix: Transmissivity for planar structure

For two semi-infinite materials (specified by its dielectric functions) separated by d, the emission power at a given frequency via a TM (transverse magnetic) mode [44, 46] is

$$\begin{aligned} S_z^{(TM)}(z,\omega) &= \frac{1}{(2\pi)^3}\hbar\omega\Theta(\omega,T)\left(\frac{\omega}{c}\right)^2 \times \\ & \int \frac{d^2\mathbf{K}}{(\omega/c)^2}\frac{1}{|\alpha_{TM}|^2}\frac{\mathrm{Re}[\tilde{\gamma}_0]\mathrm{Re}[\gamma_2]}{(\omega/c)^2}\left(1+\frac{k^2}{|\gamma_2|^2}\right)e^{+2\mathrm{Im}[\gamma_0](z-d)}. \end{aligned} \tag{28}$$

Here α_{TM} is defined as

$$\alpha_{TM} \equiv \frac{1}{4}\left[e^{i\gamma_1 d}\left(\frac{\tilde{\gamma}_0}{\tilde{\gamma}_2}+\frac{\tilde{\gamma}_0}{\tilde{\gamma}_1}+\frac{\tilde{\gamma}_1}{\tilde{\gamma}_2}+1\right)+e^{-i\gamma_1 d}\left(\frac{\tilde{\gamma}_0}{\tilde{\gamma}_2}-\frac{\tilde{\gamma}_0}{\tilde{\gamma}_1}-\frac{\tilde{\gamma}_1}{\tilde{\gamma}_2}+1\right)\right], \quad (29)$$

with $\tilde{\gamma}_i = \frac{\gamma_i}{\epsilon_i}$, $k^2+\gamma_i^2 = \epsilon_i(\frac{\omega}{c})^2$. The total emitting power (integrating over all frequency) is

$$\begin{aligned} S &= \int d\omega S_z^{(TM)}(z=d,\omega) \\ &= \int \frac{d\omega}{2\pi}\hbar\omega\Theta(\omega,T)\times \\ &\quad \left[\left(\frac{\omega}{c}\right)^2\frac{1}{(2\pi)^2}\int\frac{d^2\mathbf{K}}{(\omega/c)^2}\frac{1}{|\alpha_{TM}|^2}\frac{\mathrm{Re}[\tilde{\gamma}_0]\mathrm{Re}[\gamma_2]}{(\omega/c)^2}\left(1+\frac{k^2}{|\gamma_2|^2}\right)\right] \\ &= \int \frac{d\omega}{2\pi}\hbar\omega\Theta(\omega,T)\left[\frac{d^2\mathbf{K}}{(2\pi)^2}\varepsilon_{12}(\omega,\mathbf{K})\right] \end{aligned} \quad (30)$$

Note that in Eq. 30, the term in the square bracket has the dimension $1/L^2$, and the dimensionless transmissivity at a given in-plane $\mathbf{K}$ and frequency ω is give by

$$\varepsilon_{12}(\omega,\mathbf{K}) = \frac{1}{|\alpha_{TM}|^2}\frac{\mathrm{Re}[\tilde{\gamma}_0]\mathrm{Re}[\gamma_2]}{(\omega/c)^2}\left(1+\frac{k^2}{|\gamma_2|^2}\right). \quad (31)$$

Eq. 31 is the transmissivity for two planar reservoirs. Let us consider the vacuum case, where $\epsilon_0=\epsilon_2=1$ so $\tilde{\gamma}=\gamma$. In this case, $|\alpha_{TM}|^2=1$, and $1+\frac{k^2}{|\gamma_2|^2} = \frac{(\omega/c)^2}{|\gamma_2|^2}$. As Eq. 31 vanishes when $\mathrm{Re}[\gamma]=0$, we obtain $\varepsilon_{12}(\omega,\mathbf{K}) = \Theta(\omega/c-|\mathbf{K}|)$, which is the formula for the blackbody radiation.

[1] W. Shockley, H. J. Queisser, Detailed balance limit of efficiency of p-n junction solar cells, Journal of Applied Physics 32 (1961) 510–519. doi:10.1063/1.1736034.

[2] N.-P. Harder, P. Würfel, Theoretical limits of thermophotovoltaic solar energy conversion, Semiconductor Science and Technology 18 (5) (2003) S151.
URL http://stacks.iop.org/0268-1242/18/i=5/a=303

[3] P. Würfel, Physics of Solar Cells, Wiley-vch, 2005.

[4] R. Strandberg, Theoretical efficiency limits for thermoradiative energy conversion, Journal of Applied Physics 117 (5) (2015) 055105. arXiv:http://dx.doi.org/10.1063/1.4907392, doi:10.1063/1.4907392.
URL http://dx.doi.org/10.1063/1.4907392

[5] R. Strandberg, Heat to electricity conversion by cold carrier emissive energy harvesters, Journal of Applied Physics 118 (21) (2015) 215102. arXiv:http://dx.doi.org/10.1063/1.4936614, doi:10.1063/1.4936614.
URL http://dx.doi.org/10.1063/1.4936614

[6] P. Santhanam, S. Fan, Thermal-to-electrical energy conversion by diodes under negative illumination, Phys. Rev. B 93 (2016) 161410. doi:10.1103/PhysRevB.93.161410.
URL http://link.aps.org/doi/10.1103/PhysRevB.93.161410

[7] W.-C. Hsu, J. K. Tong, B. Liao, Y. Huang, S. V. Boriskina, G. Chen, Entropic and near-field improvements of thermoradiative cells, Scientific Reports 6 (2016/10/13/online) 34837. doi:10.1038/srep34837.
URL http://dx.doi.org/10.1038/srep34837

[8] K. Chen, P. Santhanam, S. Sandhu, L. Zhu, S. Fan, Heat-flux control and solid-state cooling by regulating chemical potential of photons in near-field electromagnetic heat transfer, Phys. Rev. B 91 (2015) 134301. doi:10.1103/PhysRevB.91.134301.
URL http://link.aps.org/doi/10.1103/PhysRevB.91.134301

[9] P. Santhanam, D. J. Gray, R. J. Ram, Thermoelectrically pumped light-emitting diodes operating above unity efficiency, Phys. Rev. Lett. 108 (2012) 097403. doi:10.1103/PhysRevLett.108.097403.
URL http://link.aps.org/doi/10.1103/PhysRevLett.108.097403

[10] X. Liu, Z. M. Zhang, High-performance electroluminescent refrigeration enabled by photon tunneling, Nano Energy 26 (2016) 353 – 359. doi:http://dx.doi.org/10.1016/j.nanoen.2016.05.049.
URL //www.sciencedirect.com/science/article/pii/S2211285516301781

[11] G. C. Dousmanis, C. W. Mueller, H. Nelson, K. G. Petzinger, Evidence of refrigerating action by means of photon emission in semiconductor diodes, Phys. Rev. 133 (1964) A316–A318. doi:10.1103/PhysRev.133.A316.
URL `http://link.aps.org/doi/10.1103/PhysRev.133.A316`

[12] P. Berdahl, V. Malyutenko, T. Morimoto, Negative luminescence of semiconductors, Infrared Physics 29 (2-4) (1989) 667–672. doi:http://dx.doi.org/10.1016/0020-0891(89)90107-3.
URL `//www.sciencedirect.com/science/article/pii/0020089189901073`

[13] T. Ashley, C. Elliott, N. Gordon, R. Hall, A. Johnson, G. Pryce, Negative luminescence from in1xalxsb and cdxhg1xte diodes, Infrared Physics & Technology 36 (7) (1995) 1037–1044. doi:http://dx.doi.org/10.1016/1350-4495(95)00043-7.
URL `//www.sciencedirect.com/science/article/pii/1350449595000437`

[14] K. Chen, P. Santhanam, S. Fan, Near-field enhanced negative luminescent refrigeration, Phys. Rev. Applied 6 (2016) 024014. doi:10.1103/PhysRevApplied.6.024014.
URL `https://link.aps.org/doi/10.1103/PhysRevApplied.6.024014`

[15] J. Oksanen, J. Tulkki, Thermophotonic heat pump – a theoretical model and numerical simulations, Journal of Applied Physics 107 (9) (2010) 093106. arXiv:http://dx.doi.org/10.1063/1.3419716, doi:10.1063/1.3419716.
URL `http://dx.doi.org/10.1063/1.3419716`

[16] A. Narayanaswamy, G. Chen, Surface modes for near field thermophotovoltaics, Applied Physics Letters 82 (20) (2003) 3544–3546. doi:http://dx.doi.org/10.1063/1.1575936.
URL `http://scitation.aip.org/content/aip/journal/apl/82/20/10.1063/1.1575936`

[17] J. I. Watjen, X. L. Liu, B. Zhao, Z. M. Zhang, A computational simulation of using tungsten gratings in near-field thermophotovoltaic devices, ASME 2016 5th International Conference on Micro/Nanoscale Heat and Mass Transfer - Biopolis, Singapore. Volume 1: Micro/Nanofluidics

and Lab-on-a-Chip; Nanofluids; Micro/Nanoscale Interfacial Transport Phenomena; Micro/Nanoscale Boiling and Condensation Heat Transfer; Micro/Nanoscale Thermal Radiation; Micro/Nanoscale Energy Devices and Systems.

[18] X. Liu, L. Wang, Z. M. Zhang, Near-field thermal radiation: Recent progress and outlook, Nanoscale and Microscale Thermophysical Engineering 19 (2) (2015) 98–126. doi:10.1080/15567265.2015.1027836.
URL http://dx.doi.org/10.1080/15567265.2015.1027836

[19] B. Song, A. Fiorino, E. Meyhofer, P. Reddy, Near-field radiative thermal transport: From theory to experiment, AIP Advances 5 (5) (2015) 053503. doi:10.1063/1.4919048.
URL http://dx.doi.org/10.1063/1.4919048

[20] P. Davies, A. Luque, Solar thermophotovoltaics: brief review and a new look, Solar Energy Materials and Solar Cells 33 (1) (1994) 11 – 22. doi:http://dx.doi.org/10.1016/0927-0248(94)90284-4.
URL http://www.sciencedirect.com/science/article/pii/0927024894902844

[21] P. Bermel, M. Ghebrebrhan, W. Chan, Y. X. Yeng, M. Araghchini, R. Hamam, C. H. Marton, K. F. Jensen, M. Soljačić, J. D. Joannopoulos, S. G. Johnson, I. Celanovic, Design and global optimization of high-efficiency thermophotovoltaic systems, Opt. Express 18 (S3) (2010) A314–A334. doi:10.1364/OE.18.00A314.
URL http://www.opticsexpress.org/abstract.cfm?URI=oe-18-103-A314

[22] Y. X. Yeng, W. R. Chan, V. Rinnerbauer, J. D. Joannopoulos, M. Soljačić, I. Celanovic, Performance analysis of experimentally viable photonic crystal enhanced thermophotovoltaic systems, Opt. Express 21 (S6) (2013) A1035–A1051. doi:10.1364/OE.21.0A1035.
URL http://www.opticsexpress.org/abstract.cfm?URI=oe-21-106-A1035

[23] A. Lenert, D. M. Bierman, Y. Nam, W. R. Chan, I. Celanović, M. Soljacic, E. N. Wang, A nanophotonic solar thermophotovoltaic device, Nat Nano 9 (2014) 126–130. doi:10.1038/nnano.2013.286.
URL http://dx.doi.org/10.1038/nnano.2013.286

[24] D. M. Bierman, A. Lenert, W. R. Chan, B. Bhatia, I. Celanović, M. Soljacic, E. N. Wang, Enhanced photovoltaic energy conversion using thermally based spectral shaping, Nature Energy 1 (2016) 16068. doi:10.1038/nenergy.2016.68.
URL http://dx.doi.org/10.1038/nenergy.2016.68

[25] R. S. DiMatteo, P. Greiff, S. L. Finberg, K. A. Young-Waithe, H. K. H. Choy, M. M. Masaki, C. G. Fonstad, Enhanced photogeneration of carriers in a semiconductor via coupling across a nonisothermal nanoscale vacuum gap, Applied Physics Letters 79 (12) (2001) 1894–1896. arXiv:http://dx.doi.org/10.1063/1.1400762, doi:10.1063/1.1400762.
URL http://dx.doi.org/10.1063/1.1400762

[26] M. Laroche, R. Carminati, J.-J. Greffet, Near-field thermophotovoltaic energy conversion, Journal of Applied Physics 100 (6) (2006) 063704. doi:10.1063/1.2234560.
URL http://dx.doi.org/10.1063/1.2234560

[27] S. Basu, Y.-B. Chen, Z. M. Zhang, Microscale radiation in thermophotovoltaic devices – a review, International Journal of Energy Research 31 (6-7) (2007) 689–716. doi:10.1002/er.1286.
URL http://dx.doi.org/10.1002/er.1286

[28] M. Francoeur, R. Vaillon, M. P. Meng, Thermal impacts on the performance of nanoscale-gap thermophotovoltaic power generators, IEEE Transactions on Energy Conversion 26 (2) (2011) 686–698. doi:10.1109/TEC.2011.2118212.

[29] O. Ilic, M. Jablan, J. D. Joannopoulos, I. Celanovic, M. Soljačić, Overcoming the black body limit in plasmonic and graphene near-field thermophotovoltaic systems, Opt. Express 20 (S3) (2012) A366–A384. doi:10.1364/OE.20.00A366.
URL http://www.opticsexpress.org/abstract.cfm?URI=oe-20-103-A366

[30] R. Messina, P. Ben-Abdallah, Graphene-based photovoltaic cells for near-field thermal energy conversion, Scientific Reports 3 (2013) 1383.

doi:10.1038/srep01383.
URL http://dx.doi.org/10.1038/srep01383

[31] T. J. Bright, L. P. Wang, Z. M. Zhang, Performance of near-field thermophotovoltaic cells enhanced with a backside reflector, Journal of Heat Transfer 136 (2014) 062701–1.

[32] A. Karalis, J. D. Joannopoulos, squeezing near-field thermal emission for ultra-efficient high-power thermophotovoltaic conversion, Scientific Reports 6 (28472). doi:10.1038/srep28472.
URL http://dx.doi.org/10.1038/srep28472

[33] A. Karalis, J. D. Joannopoulos, Temporal coupled-mode theory model for resonant near-field thermophotovoltaics, Applied Physics Letters 107 (14). doi:http://dx.doi.org/10.1063/1.4932520.
URL http://scitation.aip.org/content/aip/journal/apl/107/14/10.1063/1.4932520

[34] A. W. Snyder, Coupled-mode theory for optical fibers, J. Opt. Soc. Am. 62 (11) (1972) 1267–1277. doi:10.1364/JOSA.62.001267.
URL http://www.osapublishing.org/abstract.cfm?URI=josa-62-11-1267

[35] W.-P. Huang, Coupled-mode theory for optical waveguides: an overview, J. Opt. Soc. Am. A 11 (3) (1994) 963–983. doi:10.1364/JOSAA.11.000963.
URL http://josaa.osa.org/abstract.cfm?URI=josaa-11-3-963

[36] H. A. Haus, W. Huang, Coupled-mode theory, Proceedings of the IEEE 79 (10) (1991) 1505–1518. doi:10.1109/5.104225.

[37] L. Zhu, S. Sandhu, C. Otey, S. Fan, M. B. Sinclair, T. Shan Luk, Temporal coupled mode theory for thermal emission from a single thermal emitter supporting either a single mode or an orthogonal set of modes, Applied Physics Letters 102 (10). doi:http://dx.doi.org/10.1063/1.4794981.
URL http://scitation.aip.org/content/aip/journal/apl/102/10/10.1063/1.4794981

[38] H. Chalabi, E. Hasman, M. L. Brongersma, An ab-initio coupled mode theory for near field radiative thermal transfer, Opt. Express 22 (24)

(2014) 30032–30046. doi:10.1364/OE.22.030032.
URL http://www.opticsexpress.org/abstract.cfm?URI=oe-22-24-30032

[39] C. Lin, B. Wang, K. H. Teo, P. Bandaru, Application of impedance matching for enhanced transmitted power in a thermophotovoltaic system, Phys. Rev. Applied 7 (2017) 034003. doi:10.1103/PhysRevApplied.7.034003.
URL https://link.aps.org/doi/10.1103/PhysRevApplied.7.034003

[40] C. Lin, B. Wang, K. H. Teo, Z. Zhang, Near-field enhancement of thermoradiative devices, Journal of Applied Physics 122 (14) (2017) 143102. arXiv:https://doi.org/10.1063/1.5007036, doi:10.1063/1.5007036.
URL https://doi.org/10.1063/1.5007036

[41] P. Würfel, The chemical potential of radiation, Journal of Physics C: Solid State Physics 15 (18) (1982) 3967.
URL http://stacks.iop.org/0022-3719/15/i=18/a=012

[42] B. Feuerbacher, P. Würfel, Verification of a generalised Planck law by investigation of the emission from gaas luminescent diodes, Journal of Physics: Condensed Matter 2 (16) (1990) 3803.
URL http://stacks.iop.org/0953-8984/2/i=16/a=010

[43] P. Würfel, S. Finkbeiner, E. Daub, Generalized Planck's radiation law for luminescence via indirect transitions, Applied Physics A 60 (1) (1995) 67–70. doi:10.1007/BF01577615.
URL http://dx.doi.org/10.1007/BF01577615

[44] D. Polder, M. Van Hove, Theory of radiative heat transfer between closely spaced bodies, Phys. Rev. B 4 (1971) 3303–3314. doi:10.1103/PhysRevB.4.3303.
URL http://link.aps.org/doi/10.1103/PhysRevB.4.3303

[45] A. A. Maradudin, D. L. Mills, Scattering and absorption of electromagnetic radiation by a semi-infinite medium in the presence of surface roughness, Phys. Rev. B 11 (1975) 1392–1415. doi:10.1103/PhysRevB.11.1392.
URL http://link.aps.org/doi/10.1103/PhysRevB.11.1392

[46] K. Joulain, J.-P. Mulet, F. Marquier, R. Carminati, J.-J. Greffet, Surface electromagnetic waves thermally excited: Radiative heat transfer, coherence properties and casimir forces revisited in the near field, Surface Science Reports 57 (34) (2005) 59 – 112. doi:http://dx.doi.org/10.1016/j.surfrep.2004.12.002.
URL `http://www.sciencedirect.com/science/article/pii/S0167572905000105`

[47] H. B. Callen, T. A. Welton, Irreversibility and generalized noise, Phys. Rev. 83 (1951) 34–40. doi:10.1103/PhysRev.83.34.
URL `http://link.aps.org/doi/10.1103/PhysRev.83.34`

[48] K. E. Dorfman, D. V. Voronine, S. Mukamel, M. O. Scully, Photosynthetic reaction center as a quantum heat engine, Proceedings of the National Academy of Sciences 110 (8) (2013) 2746–2751. arXiv:http://www.pnas.org/content/110/8/2746.full.pdf, doi:10.1073/pnas.1212666110.
URL `http://www.pnas.org/content/110/8/2746.abstract`

[49] C. Creatore, M. A. Parker, S. Emmott, A. W. Chin, Efficient biologically inspired photocell enhanced by delocalized quantum states, Phys. Rev. Lett. 111 (2013) 253601. doi:10.1103/PhysRevLett.111.253601.
URL `http://link.aps.org/doi/10.1103/PhysRevLett.111.253601`

[50] N. W. Ashcroft, N. D. Mermin, Solid State Physics, Saunders College Publishing, 1976.

[51] D. A. B. Miller, C. T. Seaton, M. E. Prise, S. D. Smith, Band-gap¯resonant nonlinear refraction in iii-v semiconductors, Phys. Rev. Lett. 47 (1981) 197–200. doi:10.1103/PhysRevLett.47.197.
URL `http://link.aps.org/doi/10.1103/PhysRevLett.47.197`

[52] S. Adachi, Optical dispersion relations for GaP, GaAs, GaSb, InP, InAs, and InSb, $Al_xGa_{1-x}As$, and $In_{1-x}Ga_xAs_yP_{1-y}$, Journal of Applied Physics 66 (12) (1989) 6030–6040. arXiv:http://dx.doi.org/10.1063/1.343580, doi:10.1063/1.343580.
URL `http://dx.doi.org/10.1063/1.343580`

[53] D. E. Aspnes, A. A. Studna, Dielectric functions and optical parameters of Si, Ge, GaP, GaAs, GaSb, InP, InAs, and InSb from 1.5 to 6.0 ev, Phys. Rev. B 27 (1983) 985–1009. doi:10.1103/PhysRevB.27.985.
URL http://link.aps.org/doi/10.1103/PhysRevB.27.985

[54] S. Adachi, Model dielectric constants of GaP, GaAs, GaSb, InP, InAs, and InSb, Phys. Rev. B 35 (1987) 7454–7463. doi:10.1103/PhysRevB.35.7454.
URL http://link.aps.org/doi/10.1103/PhysRevB.35.7454

[55] R. S. DiMatteo, P. Greiff, S. L. Finberg, K. A. YoungWaithe, H. K. H. Choy, M. M. Masaki, C. G. Fonstad, Microngap thermophotovoltaics (mtpv), AIP Conference Proceedings 653 (1) (2003) 232–240. doi:http://dx.doi.org/10.1063/1.1539379.
URL http://scitation.aip.org/content/aip/proceeding/aipcp/10.1063/1.1539379

[56] R. DiMatteo, P. Greiff, D. Seltzer, D. Meulenberg, E. Brown, E. Carlen, K. Kaiser, S. Finberg, H. Nguyen, J. Azarkevich, P. Baldasaro, J. Beausang, L. Danielson, M. Dashiell, D. DePoy, H. Ehsani, W. Topper, K. Rahner, R. Siergiej, Microngap thermophotovoltaics (mtpv), AIP Conference Proceedings 738 (1) (2004) 42–51. doi:http://dx.doi.org/10.1063/1.1841878.
URL http://scitation.aip.org/content/aip/proceeding/aipcp/10.1063/1.1841878

[57] J. I. Watjen, B. Zhao, Z. M. Zhang, Near-field radiative heat transfer between doped-si parallel plates separated by a spacing down to 200nm, Applied Physics Letters 109 (20) (2016) 203112. arXiv:https://doi.org/10.1063/1.4967384, doi:10.1063/1.4967384.
URL https://doi.org/10.1063/1.4967384

[58] G. Bauhuis, P. Mulder, E. Haverkamp, J. Huijben, J. Schermer, 26.1% thin-film gaas solar cell using epitaxial lift-off, Solar Energy Materials and Solar Cells 93. doi:10.1016/j.solmat.2009.03.027.

[59] S. W. Bedell, K. Fogel, P. Lauro, D. Shahrjerdi, J. A. Ott, D. Sadana, Layer transfer by controlled spalling, Journal of Physics D: Applied

Physics 46 (15) (2013) 152002.
URL http://stacks.iop.org/0022-3727/46/i=15/a=152002

[60] C.-W. Cheng, K.-T. Shiu, N. Li, S.-J. Han, L. Shi, D. K. Sadana, Epitaxial lift-off process for gallium arsenide substrate reuse and flexible electronics, Nature Communications 4. doi:10.1038/ncomms2583.

[61] L. Riuttanen, P. Kivisaari, H. Nyknen, O. Svensk, S. Suihkonen, J. Oksanen, J. Tulkki, M. Sopanen, Diffusion injected multi-quantum well light-emitting diode structure, Applied Physics Letters 104. doi:10.1063/1.4866343.

[62] L. Riuttanen, P. Kivisaari, O. Svensk, J. Oksanen, S. Suihkonen, Electrical injection to contactless near-surface ingan quantum well, Applied Physics Letters 107. doi:10.1063/1.4928248.

[63] P. Riuttanen, Lauri; Kivisaari, O. Svensk, J. Oksanen, S. Suihkonen, Diffusion injection in a buried multiquantum well light-emitting diode structure, IEEE Transactions on Electron Devices 62. doi:10.1109/ted.2015.2391117.

[64] P. Kivisaari, I. Kim, S. Suihkonen, J. Oksanen, Elimination of lateral resistance and current crowding in large-area leds by composition grading and diffusion-driven charge transport, Advanced Electronic Materials-doi:10.1002/aelm.201700103.

Function	Type	$(\mu, -I_c)$	description
PG	PV	$(+,-)$	low-T cell provides usable work
PG	TR	$(-,+)$	high-T cell provides usable work
Cooler	EL	$(+,+)$	work done to the to-be-cooled object
Cooler	Negative EL	$(-,-)$	work done to the heat sink

Table 1: Summary of four devices. $(\mu, -I_c)$ gives the signs of the photon chemical potential and the "negative" of the photocurrent for the device working region. PG stands for power generator. The sign of product $-I_c\mu$ determines its function: negative corresponds to power generators; positive corresponds to cooling devices.

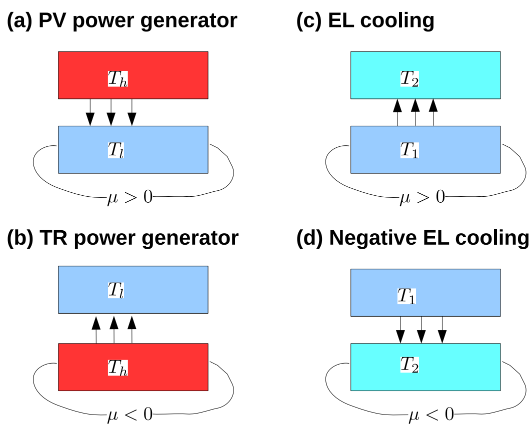

Figure 1: (a) The PV cell as a power generator: the power is generated via the low-T PV cell. (b) The TR cell as a power generator: the power is generated via the high-T TR cell. (c) The EL cooling device. A forward bias is applied to the object 1 (at T_1) we want to cool. (d) The negative EL cooling device. A reverse bias is applied to the heat sink (at T_2). The arrows indicate the net photon flux.

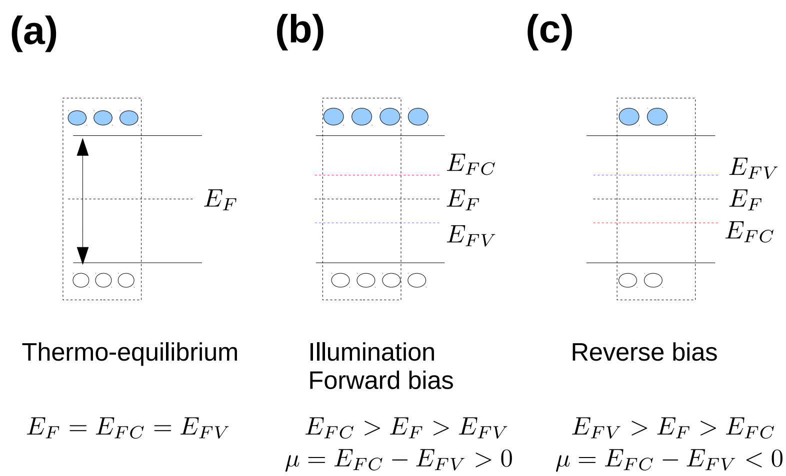

Figure 2: Illustration of the relationship between the photon chemical potential μ, the (quasi) electron/hole Fermi energies E_{FC}/E_{FV}, and the equilibrium Fermi energy E_F. The box indicates the number of electron-hole pairs at thermal equilibrium. (a) At thermal equilibrium, $E_F = E_{FC} = E_{FV}$, and $\mu = E_{FC} - E_{FV} = 0$. (b) In the non-equilibrium situation where e-h concentration is larger than that at equilibrium, $E_{FC} > E_F$, $E_{FV} < E_F$ and $\mu = E_{FC} - E_{FV} > 0$. (c) In the non-equilibrium situation where e-h concentration is smaller than that at equilibrium, $E_{FC} < E_F$, $E_{FV} > E_F$, and $\mu = E_{FC} - E_{FV} < 0$.

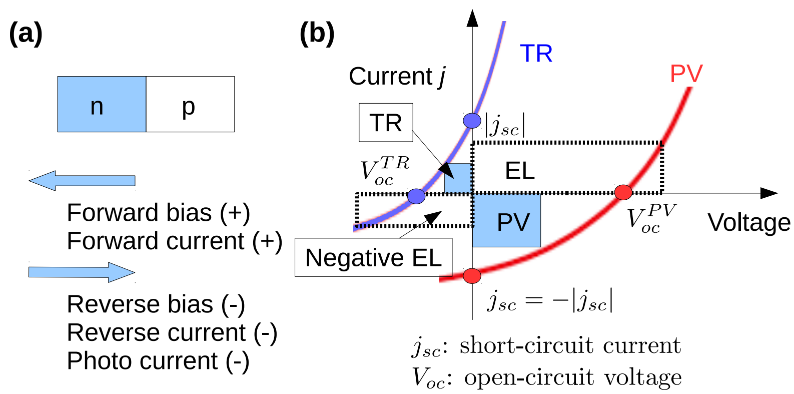

Figure 3: (a) The sign convention of a pn-junction. Forward-bias voltage and current directions are chosen to be '+'; reverse-bias voltage and current directions '-'. (b) Current-voltage relation for PV (red) and TR (blue) cells. The blue shaded areas represent the power delivered by the PV and TR devices: the larger area gives the larger output power. The areas of dashed boxes represent the work done to the EL and negative EL devices: the smaller area gives the better cooling performance. The rectangular areas are randomly chosen and for illustration only.

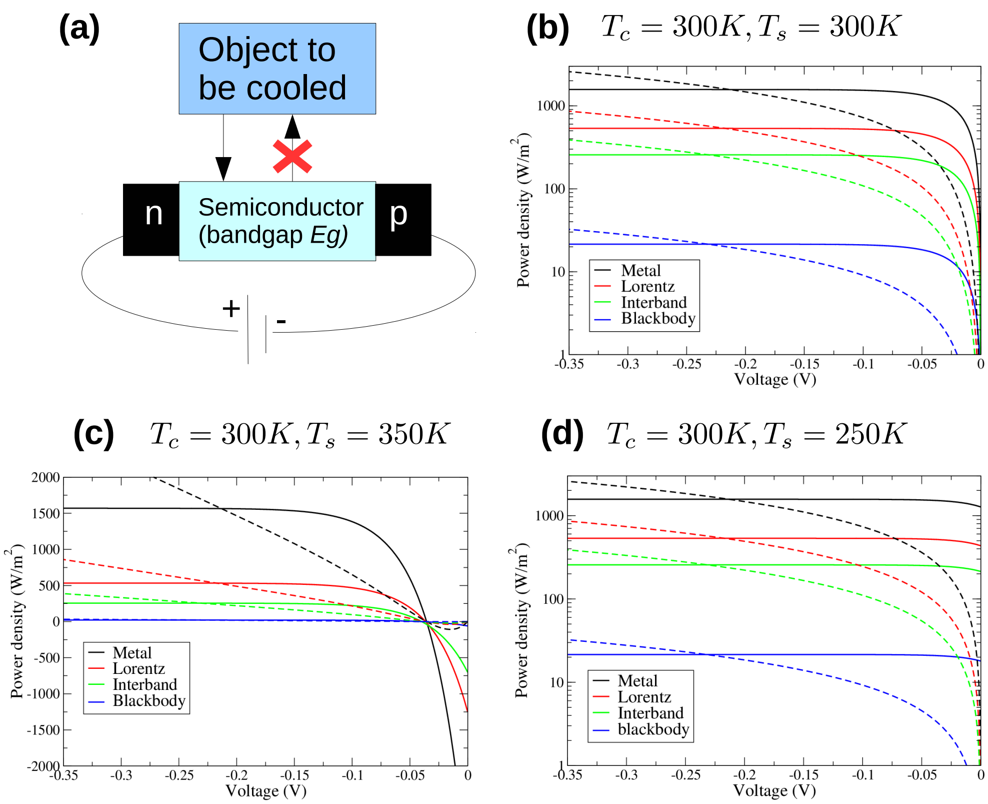

Figure 4: (a) The illustration of negative EL device. The heat sink is a semiconductor of a bandgap E_g. When a reverse bias voltage is applied, the heat sink emits much less photons (the arrows with a red cross), effectively enhancing the heat removal flux of the object one wants to cool. (b)-(d) The input power (dashed curves) and the outgoing radiative flux (solid curves) per unit area of the metal (black), Lorentz (red), interband (green) target cells, with blackbody reference (blue). The heat sink temperature is T_s, whereas the cell temperature is T_c. (b) $T_c = 300$K, $T_s = 300$ K. (c) $T_c = 300$ K, $T_s = 350$ K (beware of the linear scale in power density) (d) $T_c = 300$ K, $T_s = 250$ K. When the applied voltage is large in amplitude, the outgoing heat flux saturates.

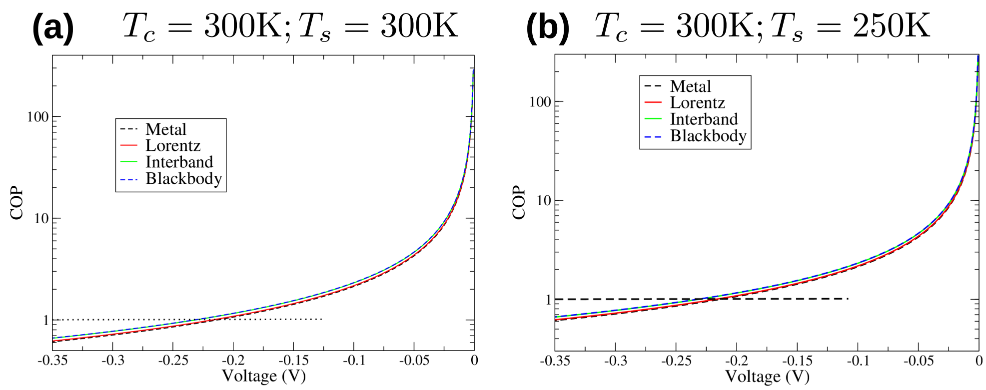

Figure 5: COP for the metal (black), Lorentz (red), interband (green) target cells, with blackbody reference (blue). (a) The cell and sink are both fixed at 300 K; (b) The cell is fixed at 300 K whereas and heat sink temperatures 250 K. The target cells that support surface resonances, i.e., metal and Lorentz, have a COP about 5% lower than those that do not support surface resonances, i.e., interband and blackbody. The dashed horizontal line represents $\eta_{COP} = 1$.

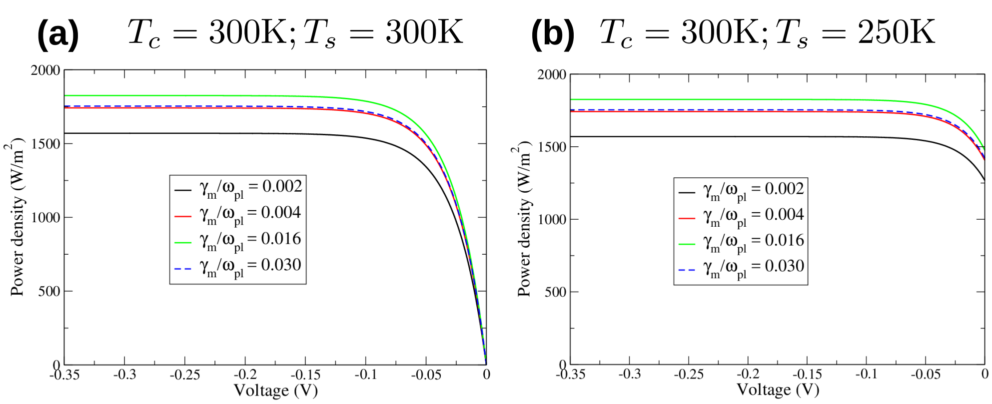

Figure 6: The outgoing radiative flux (in linear scale) per unit area for the metals of plasma damping rate $\gamma_e/\omega_{pl} = 0.002$ (black), 0.004 (red), 0.016 (green), and 0.030 (blue). (a) The cell and sink are both fixed at 300 K; (b) The cell is fixed at 300 K whereas and heat sink temperatures 250 K. The radiative flux shows a maximum value when $\gamma_m/\omega_{pl} \sim 0.016$ for both temperature differences.